A variable stiffness mechanism for steerable percutaneous instruments
Integration in a needle

de Falco, Iris; Culmone, Costanza; Menciassi, Arianna; Dankelman, Jenny; van Den Dobbelsteen, John J.

DOI
10.1007/s11517-018-1847-7

Publication date
2018

Document Version
Final published version

Published in
Medical and Biological Engineering and Computing

Citation (APA)
de Falco, I., Culmone, C., Menciassi, A., Dankelman, J., & van Den Dobbelsteen, J. J. (2018). A variable stiffness mechanism for steerable percutaneous instruments: Integration in a needle. *Medical and Biological Engineering and Computing*, *56*(12), 2185-2199. https://doi.org/10.1007/s11517-018-1847-7

Medical & Biological Engineering & Computing (2018) 56:2185–2199
https://doi.org/10.1007/s11517-018-1847-7

ORIGINAL ARTICLE

A variable stiffness mechanism for steerable percutaneous instruments: integration in a needle

Iris De Falco[1] · Costanza Culmone[2] · Arianna Menciassi[1] · Jenny Dankelman[2] · John J. van den Dobbelsteen[2]

Received: 21 August 2017 / Accepted: 16 May 2018 / Published online: 4 June 2018

Abstract
Needles are advanced tools commonly used in minimally invasive medical procedures. The accurate manoeuvrability of flexible needles through soft tissues is strongly determined by variations in tissue stiffness, which affects the needle-tissue interaction and thus causes needle deflection. This work presents a variable stiffness mechanism for percutaneous needles capable of compensating for variations in tissue stiffness and undesirable trajectory changes. It is composed of compliant segments and rigid plates alternately connected in series and longitudinally crossed by four cables. The tensioning of the cables allows the omnidirectional steering of the tip and the stiffness tuning of the needle. The mechanism was tested separately under different working conditions, demonstrating a capability to exert up to 3.6 N. Afterwards, the mechanism was integrated into a needle, and the overall device was tested in gelatine phantoms simulating the stiffness of biological tissues. The needle demonstrated the capability to vary deflection (from 11.6 to 4.4 mm) and adapt to the inhomogeneity of the phantoms (from 21 to 80 kPa) depending on the activation of the variable stiffness mechanism.

Keywords Minimally invasive instruments · Steerable needle · Needle deflection · Tissue inhomogeneity · Variable stiffness

1 Introduction

Minimally invasive interventions are often based on percutaneous diagnosis and local therapies, in which needles, catheters or probes are inserted into soft and inhomogeneous tissues to reach a target [1]. Needles are very common tools, which can be used for biopsies [2], regional anaesthesia, fluid sampling [3], neurosurgery [4], and brachytherapy [5] and for the introduction of catheters, ablation electrodes or other instruments into the body [6]. In many of these procedures, the final tip placement accuracy is crucial for a successful clinical outcome (i.e., biopsy taking, ablation). In a typical intervention, the target lies in line with the needle, but several factors such as human tremor; imaging limitations; displacement of the target because of breathing, swelling or heartbeat [7]; tissue deformation and needle deflection can lead to alignment errors. Tissue deformation is directly dependent on the mechanical properties of the soft tissues, while needle deflection is caused by the flexibility of a long needle when it passes through the biological tissues [8, 9].

Due to needle tip misplacement, malignancies could not be detected during biopsy, radioactive seeds could not be deposited in the correct site during brachytherapy [10], adverse effects might occur from an inaccurate anaesthesia [8], repuncturing with additional damage to the tissue could be necessary [11], or false negative cases could be detected.

A great deal of effort has already been made to improve the accuracy of needles in percutaneous interventions. For example, robotics and medical imaging can support needle procedures [12–16]: computed tomography (CT), ultrasound (US) and magnetic resonance (MR) are imaging techniques commonly used for planning, tracking and modelling an intervention. In particular, real-time imaging and real-time force feedback permit monitoring of the needle, identify tissue deformation and target displacement [17–19]. Regarding the design, a large number of needles have been conceived to allow physicians to control the steering and deflection of the instruments during insertion with the aim to accurately reach the target [20]. Basing on the mechanical parameters of the tissue and the needle, 3D steerable needles integrating real-time

✉ Iris De Falco
i.defalco@alumni.sssup.it

[1] The BioRobotics Institute, Scuola Superiore Sant'Anna, Pisa, Italy

[2] Department of BioMechanical Engineering, Delft University of Technology, Delft, The Netherlands

algorithms that automatically plan the path have been proposed [21, 22], while several studies report control of the needle deflection using duty-cycle modulation in combination with a flexible bevel tip [23, 24]. In addition, passive and active steering methods have been extensively tested to adjust the needle shape during insertion [6]. A bevel tip has been chosen in many studies that aim to predict and control the needle behaviour using path planning and design optimization [25]. Other types of programmable tips, in combination with a tendon-driven system or FBG sensors, have been designed to control the needle insertion and steering [26, 27]. Other approaches obtain precision of the path using pre-curved needles in straight stylets or integrate the system in a tendon-driven robot [28, 29]. Tissue deformation, needle deflection and needle-tissue interactions have been extensively studied in order to better control the insertion of needles [30] and estimate the relation between the applied force and the movement of both the needle and the tissue [31, 32].

Although many efforts focused on the behaviour of the needle in tissues, the differences in stiffness of biological tissues have to be taken into account for needle design. As mentioned before, the mechanical properties of the tissues affect the needle-tissue interaction and thus produce needle deflection. Indeed, a major limitation for all approaches is that extensive needle curvature demands a highly flexible needle shaft. However, in non-homogenous biological tissues, this could lead to path deviations or even buckling when stiffer tissues are encountered.

The present work extends existing needle steering approaches with the design of an adaptable stiffness needle. The aim of this study is to propose a possible solution for compensating deflection using a mechanism able to vary the stiffness in order to achieve fine adjustment and accurately reach the target. The mechanism is intended to be integrated into flexible needles for procedures in tissues where deflection can easily occur. In this work, the mechanism has been integrated into a general-purpose needle to allow needle steering. A highly flexible shaft follows the behaviour of the tip when puncturing various layers of tissue; as such, the needle is also able to maintain the intended direction when introduced into a stiffer layer. In addition, the structure of the mechanism allows for the omnidirectional steering of the tip, making it easier to approach the target. Preliminary works have been presented in [33, 34]. Here, an optimization of the device is provided, and further experimental tests are reported in order to demonstrate the working capabilities of the needle.

2 Materials

2.1 Concept and needle model

As hereinbefore mentioned, the insertion of a needle in a biological tissue depends on many factors such as the variations in stiffness of the biological structures. These can affect the needle-tissue interactions and thus the needle deflection. Figure 1a shows how a traditional needle passing through several tissues can be deflected and then misplaced with respect to the target. The steerable needle presented here was able to control the deflection and adapt its stiffness to the tissue stiffness, allowing better maintenance of the trajectory during the insertion, without missing the target (Fig. 1b). The target can actually change its position during the insertion. With a traditional needle, there is no possibility to change the pathway during the procedure (Fig. 1c); on the other hand, steerable needles allow the possibility of reaching the target even if its position has changed (Fig. 1d).

The needle presented here was designed to compensate for the additional deflection due to the passage through tissues of different stiffness. Knowing the tissue stiffness, the variable stiffness needle could compensate for the tissue stiffness

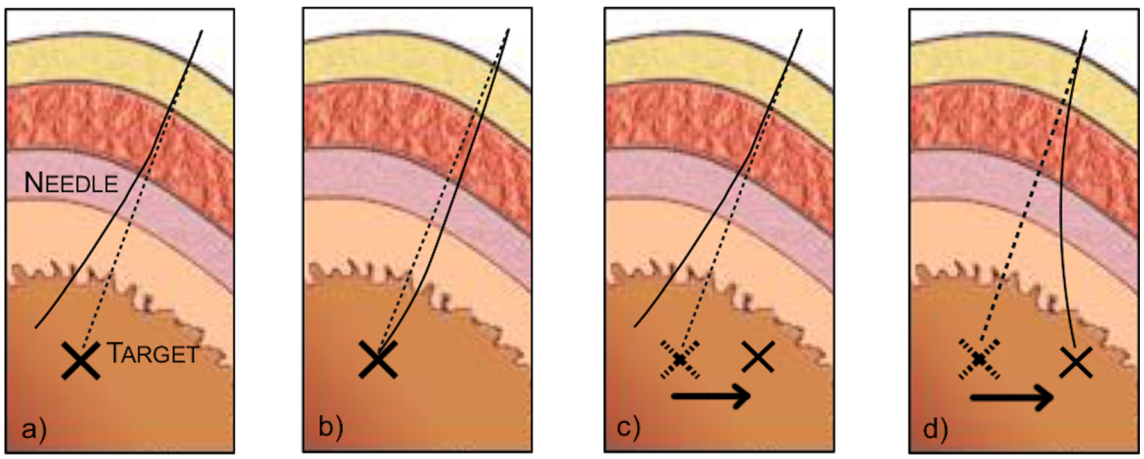

Fig. 1 Comparison between traditional needle and variable stiffness needle behaviour. **a** Deflection and missing the target by a traditional needle. **b** Behaviour of a variable stiffness needle through tissues of different stiffness. **c** Change in position of the target during the insertion with the negative deflection of the traditional needle. **d** Capability of the steerable needle to reach the target even when its position changes during the insertion of the needle

variation by changing the stiffness of the mechanism. In this early prototype, a pre-evaluation of the tissue properties was performed, and all feedback was based on the visual and direct visualisation of the tip. An overview of the device is shown in Fig. 2. The outer diameter of the needle is 3 mm, which is a value close to 3.048 mm, corresponding to an 11 gauge needle, suitable for procedures in soft tissues [32, 35, 36]. The needle is composed of the tip, variable stiffness mechanism, cannula and cables for driving the needle and tuning its stiffness. The tip can be conical or bevelled, both with the possibility of being opened or closed according to the needle application; a screw mechanism in the distal part of the device allows fixing the favoured tip. The variable stiffness mechanism is 11 mm long, and it consists of three compliant segments connected to four rigid plates.

The cannula is a steerable hollow tube, which includes four holes in the wall for the passage of the cables. Four tendons are symmetrically placed at 90° in a 2.3-mm diameter (Fig. 2b), and they pass through the variable stiffness mechanism and the cannula.

By pulling one or a combination of the tendons, the needle bends in different directions depending on the pulled cable and thus will steer in the preferred direction.

To study the precision of the mechanism, a kinematic model was formulated, taking into account the quasistatic behaviour of the needle due to the low insertion speed. The model aimed to analyse the radius of curvature of the variable stiffness mechanism. In particular, the arc of the circumference covered by the mechanism with different angles of curvature was considered.

The length of the entire mechanism is 11 mm ($L1$), as reported in Fig. 3a. $L1$ corresponds to the resting length of the cable when it is not tensioned. If a cable is pulled (Fig. 3b), the mechanism bends, and the arc of the circumference decreases in $L2$ due to the compression of the compliant parts. The final length of the cable corresponds to the part of the cable inside the mechanism ($L2$) and the cable pulled outside (ΔL).

- Assuming that the middle line (L_1) remains a constant 11 mm in length while one of the cables is pulled; and
- Knowing that the radius of the mechanism (r) is 1.5 mm (Fig. 2b);

the radius of curvature (R_1) and the angle of curvature (θ) when a cable is pulled can be calculated (Fig. 3c).

Knowing the relation between R_1, $L2$ and $R2$, it is possible to derive ΔL as follows:

$$R_1 = \frac{360 \times L_1}{2\pi\theta} \tag{1}$$

$$L_2 = \frac{\theta \times 2\pi R_2}{360} \tag{2}$$

$$R_2 = R_1 - r \tag{3}$$

$$\Delta L = L_1 - L_2 = L_1 - \frac{\theta \times 2\pi(R_{1-r})}{360} \tag{4}$$

Considering different angles of curvature, the radius of curvature and the displacement of the cables were calculated, as reported in Table 1.

The tension is applied to the cables and thus to the mechanism, which depends on the displacement imposed to the cables. Considering that the compliant parts are made of nonlinear material, the force can be approximated as:

$$F = K_{nl}\Delta L \tag{5}$$

where:

F is the tension exerted on the cable;
K_{nl} is a parameter depending on the nonlinear characteristics of the materials and geometry;
ΔL is the displacement of the tensioned cable.

In particular, the force is provided by:

$$F = K_{nl}\left(L_1 - \frac{\theta \times 2\pi(R_1 - r)}{360}\right) \tag{6}$$

This demonstrates that, when increasing the tension on cable, the radius of the curvature decreases.

To clarify the steering and the variable stiffness capabilities of the needle, the main combinations of pulled cables are reported in Table 2. If one cable (i.e., first and second cases in Table 2) is tensioned, the tip bends towards that cable; if two nearby cables are tensioned with the same tension, at 90° to each other (i.e., third case in Table 2), the tip bends on the intermediate plane between the cables, while if two nearby

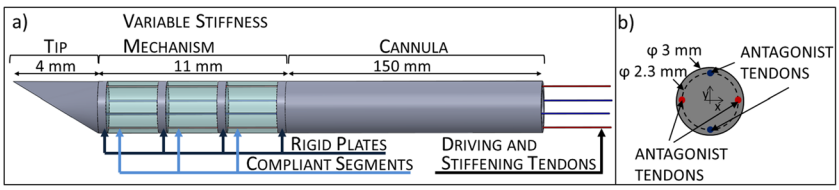

Fig. 2 **a** Overall sketch of the needle. The rigid plates are made of aluminium, while the compliant segments are made of Smooth-Sil 940 silicone (Smooth-On). **b** A cross-sectional view of the variable stiffness mechanism, where the coupling of antagonist tendons indicates the two cables, which are positioned 180 degrees from each other, inducing an opposing action

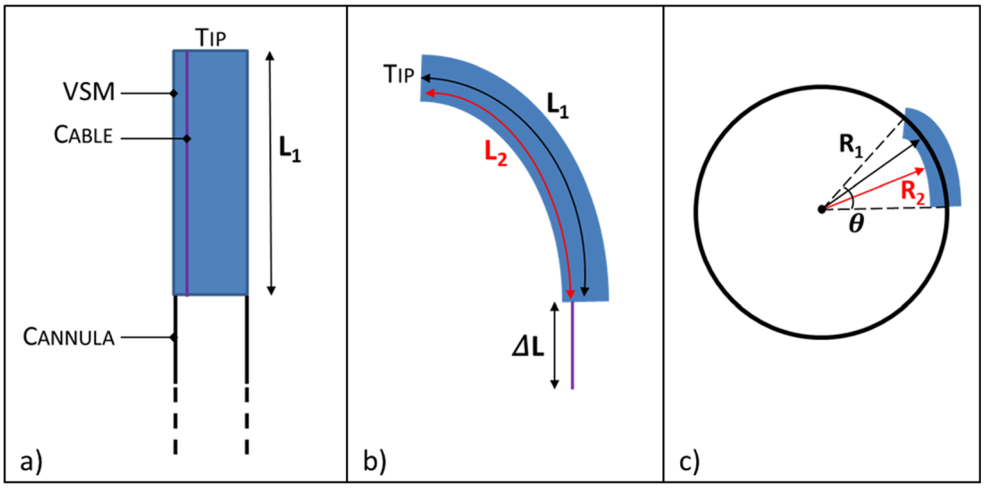

Fig. 3 Sketch of the variable stiffness mechanism (VSM) used for the kinematic model. **a** Resting position. **b** Bending. **c** Radius and angle of curvature

cables are tensioned with different tensions, the tip bends on other planes.

With regard to the variable stiffness nature of the needle, when two antagonistic cables are simultaneously pulled with the same load (i.e., fourth case in Table 2), the compliant parts of the mechanism are compressed producing an additional force; thus, the axial stiffness of the needle increases. This observation is because the property of the compliant material is nonlinear (as discussed in Section 2.2); therefore, this nonlinear property induces the variation of the stiffness in the overall system. When the tendons are released, the axial stiffness of the needle decreases. Using this characteristic, the stiffness of the device is actively changed by controlling the tendons.

One possible combination of the tendons could be the following: the stiffness of the needle could be increased by pulling with the same load on two antagonistic cables and then steering the needle using the free driving cables. It is worth mentioning that there are many possible combinations of cables that could be used in order to increase the stiffness and steer the needle. Stiffness and steering direction are coupled and cannot necessarily be independently controlled; all four cables can be used to reach the desirable stiffness and steering simultaneously. In this work, the main possible configurations were studied, and the performance in terms of stiffness were evaluated.

Table 1 Radius of curvature and displacement of the cables for different angles of curvature

θ (angle of curvature, deg)	R_1 (Radius of curvature, mm)	ΔL (displacement of the cables, mm)
10	63.06	0.26
20	31.52	0.53
30	21.02	0.78
45	14.01	1.18
50	12.61	1.31
60	10.51	1.57

2.2 Fabrication of the needle

The rigid plates of the variable stiffness mechanism are 0.5 mm long, and they are made of aluminium, while the compliant parts are 3 mm long cylinders, and they are made of Smooth-Sil 940 silicone (Smooth-On). The cannula is made by PEEK plastic (IDEX® Health & Science) and was already assessed in previous works [20, 26]. For the cables, Dyneema wires of 0.08 mm pass through the rigid and compliant parts in which four dedicated guides have been designed. Compliant and rigid parts are connected by silicone glue (Momentive, 127,374). The needle tip is 4 mm long, and it is made of aluminium. All components and specifications of the final prototype are summarised in Table 3.

Table 2 Needle motion and stiffness specifications. Red points indicate the pulled cables

Cables state	Needle behaviour
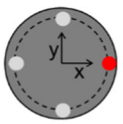	Tip bends on *x* direction
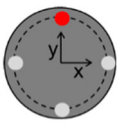	Tip bends on *y* direction
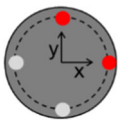	Tip bends on *xy* direction
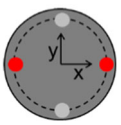	Needle increases stiffness

Table 3 Needle components and features

Needle component	# pieces	Size (length × diameter) (mm)	Material
Tip	1	4 × 3	Aluminium
Rigid plates	4	0.5 × 3	Aluminium
Compliant segments	3	3 × 3	Silicone Smooth-Sil 940 (Smooth-On)
Cannula	1	150 × 3	PEEK plastic (IDEX® Health & Science)
Cables	4	300 × 0.08	Dyneema

The Smooth-Sil 940 silicone used for designing the compliant parts has a shore hardness of 40A, which represents a suitable material in terms of application and fabrication process. Indeed, its liquid physical state before the polymerisation process permits the solution to be poured into a dedicated mould, obtaining the desired structure. The silicone has been mechanically characterised with compression tests in a tensile-compression machine (model Z005 of Zwick/Roell) at a speed of 10 mm/min. Samples were fabricated following the regulations reported in International Standard ISO 37:2005 (E) regarding rubber materials. Test pieces were tested up to a compression of 35% with respect to the initial length, thus ensuring that the working range of the variable stiffness mechanism was included. A load cell with a 1-kN end scale permitted the derivation of the force-compression curves from which the stress-strain curve was calculated, as reported in Fig. 4.

From the stress-strain behaviour, the Smooth-Sil 940 silicone exhibits approximately 1.1 MPa @ 35% compression. Considering the linear tract of the curve, the elastic modulus of the Smooth-Sil 940 silicone is 3.8 MPa.

With regard to the mechanism in Fig. 2, the elastic modulus (E) of the overall structure can be derived from composite material rules and the Reuss model [37] as follows:

$$\frac{1}{E} = 3\frac{V_{Al}}{E_{Al}} + 3\frac{V_{Sil}}{E_{Sil}} \tag{7}$$

where

V_{Al} and V_{Sil} are the volume fractions of the aluminium plates and silicone cylinders, respectively, and both of them correspond to 1/3 of the entire structure;

E_{Al} and E_{Sil} are the elastic moduli of aluminium and silicone, and they are 64 GPa and 3.8 MPa, respectively.

From (7), the elastic modulus, E, is mainly dependent on the elastic modulus of the compliant parts; thus, it is close to 3.8 MPa, ensuring the possibility to steer and stiffen the tip.

The fabrication process of the needle includes the fabrication of the variable stiffness mechanism and then, the integration with a tip and a cannula.

The compliant parts are fabricated by pouring the silicone in a dedicated mould composed of aluminium pieces shown in Fig. 5a: two Shells, two Caps including one lateral and four surface guides, and two Pins and four Channels to create cables guides.

The phases of the fabrication process are illustrated in Fig. 5b. First, one Shell is connected to Cap_1 with a Pin (phase 1); the silicone is poured in the central part of this mould, and the second Shell is connected to the other one through the Pin (phase 2); Cap_2 is inserted in the top side of the mould, and the second Pin is used to affix Cap_2 to the mould (phase 3). Finally, the Channels are inserted in the holes of the Caps already aligned due to the Pins (phase 4). After the polymerisation time, the aluminium pieces are removed, and the final result is a compliant silicone cylinder with four channels inside (phase 5).

The same process is repeated two more times to fabricate the other compliant parts.

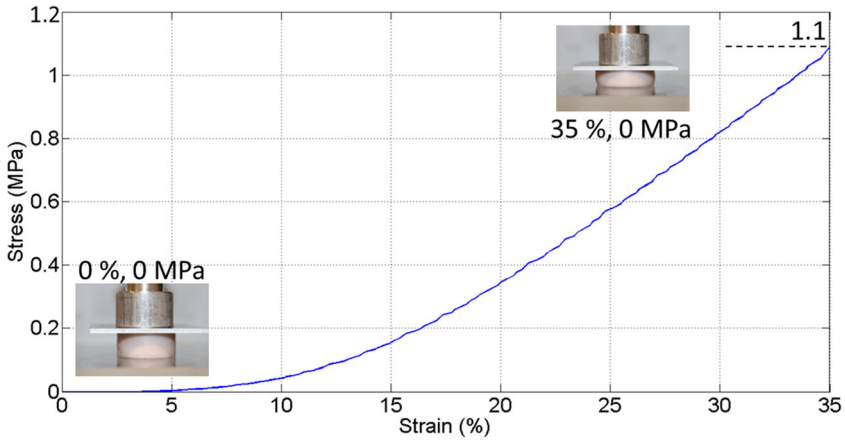

Fig. 4 Stress-strain curve of Smooth-Sil 940 silicone. In the insets, the initial and final lengths of the test piece are shown

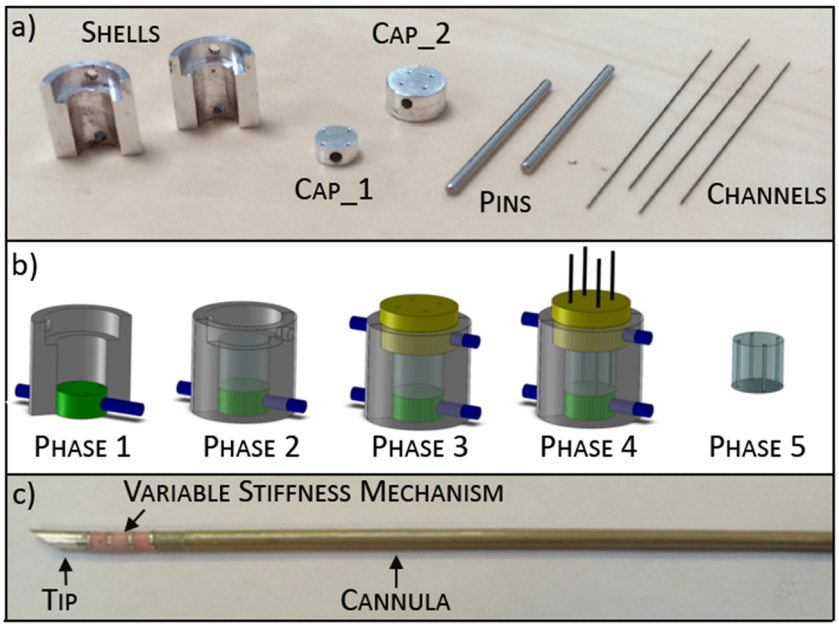

Fig. 5 **a** Pieces of the mould used to fabricate compliant parts. **b** Fabrication process of a compliant part. First, the shells, Cap_1 and a Pin are connected, and then, the silicone is poured (phase 1 and 2). Cap_2, the other Pin and Channels are inserted in the mould (phase 3 and 4), and after polymerisation, the compliant part is ready (phase 5). **c** Final prototype

Afterwards, the cables are passed through the compliant and aluminium parts, and then, the compliant segments and rigid plates are attached by gluing. Finally, the cables are passed through the cannula, while the tip is connected to the rigid plate. The final prototype is shown in Fig. 5c.

3 Methods

To study the performance of the variable stiffness of the needle, first, the capabilities of the single variable stiffness mechanism were evaluated. Afterwards, the overall needle was experimentally tested with tests aimed to study how the different stiffness of the needle influences the behaviour in gelatine.

3.1 Performance evaluation of the variable stiffness mechanism

Two different working conditions were considered, straight and curved positions, which represent two possible states of the needle during interventions. In both of the cases, the force developed by the prototype was experimentally measured, and the deformation was modelled with a finite element model (FEM).

3.1.1 Straight position

The setup used to evaluate the variable stiffness of the mechanism in the straight position is shown in Fig. 6. The prototype was fixed in a support permitting the cables to be tensioned from the bottom side. An S-beam load cell (LSB200-2 lbs, model FSH00102, ±0.1% FS accuracy, FUTEK Advanced Sensor Technology Inc., CA, USA) was linked on a linear guide, and it moved at 0.8 mm/s. The prototype was positioned in proximity to the load cell. A displacement of 2 mm (2/3 of the prototype diameter) was imposed by the load cell towards the prototype using a dedicated interface and software. The load cell allowed acquisition of the force-displacement behaviour from which the force of the mechanism could be measured. Two antagonistic cables (stiffening cables indicated by the red points in Fig. 6) were simultaneously tensioned with the same load in the range 0–17 N with steps of 1 N, while the other cables were free to move (grey points in Fig. 6). The stiffening cables coming out from the bottom side of the prototype were tensioned by loads. After each tensioning of the cables, the load cell moved towards the prototype, and data were acquired with a sampling

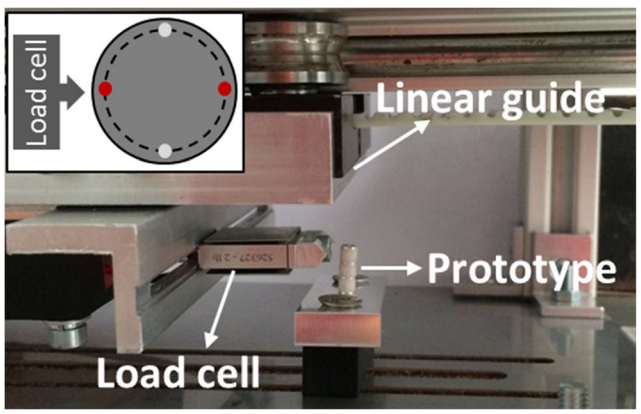

Fig. 6 Experimental setup used to evaluate the variable stiffness of the single mechanism. Cables come out from the bottom side of the prototype. In the inset, the top view of the system is shown. The stiffening cables are indicated by red points and the free cables by grey points

time of 0.1 s. Three repetitions were performed for each tension value, and then the results were averaged.

The same experimental cases were simulated using an FEM. The simulations were performed with the static structural analysis option of the Ansys Inc. software. To make the analysis coherent with the variable stiffness mechanism, the proper mechanical properties of the materials were imported in the model.

Regarding the compliant parts, the stress-strain behaviour of the silicone discussed in Fig. 4 was imported in the "materials properties" setting and then linked to the parts, while for the rigid plates, the aluminium settings available in Ansys Inc. software were used.

A structured quad-mesh with a minimum edge length of 0.50 mm was used to discretize the mechanism for an overall number of 48,124 nodes and 9309 elements. Considering the structural features of the model, bonded contacts were set between every rigid plate and the related compliant part. All tensioning states used in the experimental tests (17 tension values) were simulated as a compression force on the mechanism.

3.1.2 Curved position

The mechanism was also tested in the curved position. Indeed, during a needle intervention, the needle could bend to compensate for path deviations. To evaluate the worst case, an angle of 20° was considered (Fig. 7a); indeed, previous studies that used an actively bent tip in this range obtained high curvature [26].

The setup used to characterise the mechanism in the curved position is already shown in Fig. 6. In this case, the load cell moved towards the mechanism, orthogonally to the bending plane. One driving cable was used to set the bent position (blue point in Fig. 7b), and it was tensioned until it reached a position of 20°. The other driving cable (grey point in Fig. 7b) was free to move, while the other two antagonistic cables (stiffening cables indicated by red points) were tensioned in the range 0–17 N with steps of 1 N, as in the straight position. Additionally, in this case, the acquisition method was based on repetitive acquisitions in each tension state.

Regarding the straight position, the curved case was simulated with an FEM. The mechanical behaviour of the compliant parts and rigid plates was imported in "materials properties". A structured quad-mesh was implemented, and the bonded contacts were set between every rigid plate and the related compliant part. The prototype model was curved at 20°, and all tensioning states (17 values) were applied with a step of 1 N.

3.2 Deflection and stiffness adaptability of the needle

Once the performance of the variable stiffness mechanism was evaluated, it was integrated in the needle. The overall device was tested in two different working conditions: a one-layer phantom to analyse how the deflection changes with respect to the tension applied to the cables, and a phantom of two layers with different stiffness to estimate the capability of the needle to maintain the same trajectory in a stiffer tissue. In both the experiments, the aim was to study the behaviour of the needle when equipped with the variable stiffness mechanism. For this reason, external factors such as the presence of a membrane on the phantom surface or between phantom layers were not considered.

1.1.1. One-layer phantom tests

The setup used for the one-layer phantom experiments is shown in Fig. 8.

The needle was rigidly fixed with a support to a linear vertical stage, which provides translation in vertical direction (z-axis indicated in Fig. 8) at a constant speed. The needle support consisted of two lateral arms on which four pulleys, two for each arm, were fixed. Two antagonistic cables slid on the pulleys while loads were laterally attached to the cables for their tensioning. The other two cables were left free. Two cameras (iSight Camera, 8 MPX, 30 frames per second) were placed laterally to the phantom to acquire the needle motion during tests.

The phantom used to test the needle tried to reproduce the mechanical properties of biological tissues. It was made with a 5% (w/w) gelatine-water mixture at 70 °C and then stored at 2 °C until use [20]. Samples of 5% gelatine were mechanically characterised with compression tests using a Zwick/Roell Z005 tensile-compression machine (Zwick GmbH & Co, Germany) at a speed of 10 mm/min to a 35% compression with respect to the initial length. Figure 9 shows the stress-strain curve of 5% gelatine (red line). The elastic modulus of

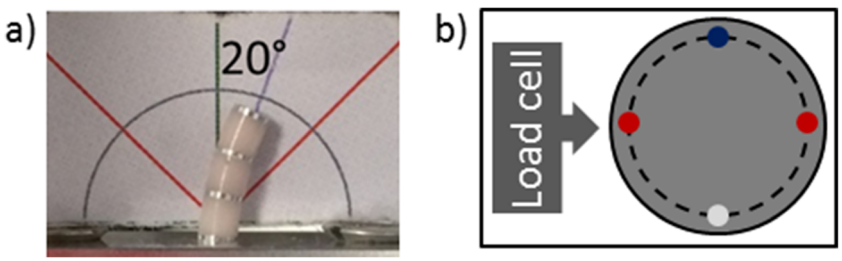

Fig. 7 **a** Curved position of the mechanism was experimentally evaluated. **b** Top view of the system. The red points represent the stiffening cables. The other two cables are the driving tendons: the blue one is tensioned to set the position, and the grey one is free to move

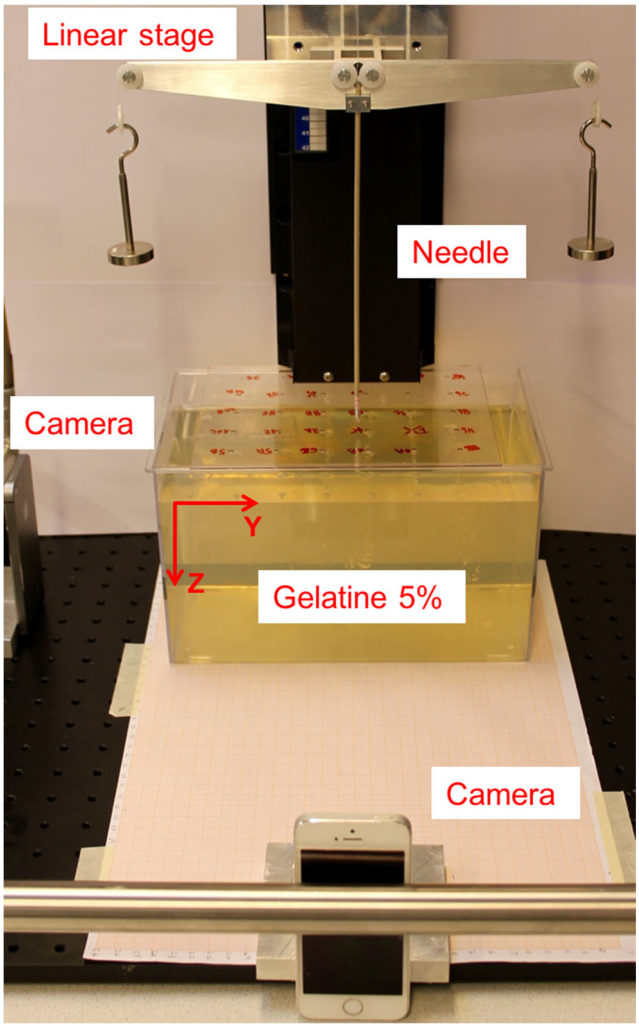

Fig. 8 Setup used to test the needle motion inside one-layer gelatine

5% gelatine was 21 kPa, which was a suitable value for the elastic modulus (stiffness) of soft tissues [38]. In Fig. 9, the stress-strain behaviour of the 7% gelatine (blue line) is also reported. This gelatine was 80 kPa in stiffness, and it was used for the two-layer phantom tests, as discussed in Section 3.2.2.

The speed of the linear stage used to test the needle in the gelatine phantom was 3 mm/s, which is one of the speeds generally used for needle characterisation in gelatine [39, 40].

The aim of these tests was to evaluate how the deflection of the needle changes with different tensions applied to the variable stiffness mechanism. As mentioned in Section 2.1, different tips can be integrated in the needle due to a screw mechanism. For these tests, a bevel tip of 30° was selected to ensure that the deflection of the needle was always on the same plane and that the natural bending occurred upon insertion into the soft tissue [41, 42].

The setup is designed to permit the insertion of the needle with the cables already aligned with the pulleys, avoiding deflection errors [41]. The stiffening cables have been tensioned in the range 0–10 N with steps of 1 N, where 10 N was considered the maximum value for the tests because the force developed at this tension is sufficient for needle operations, as discussed in Section 4.1.2.

For each different tensioning state, three repetitions were performed, and the needle was inserted in the gelatine at a displacement of 100 mm in the vertical direction. The insertion point of the needle into the phantom was changed for each repetition so the data would not be affected. In fact, the insertion of the needle forms a path that remains in the gelatine. Inserting the needle at the same point means influencing the data, as the needle would follow the previously established path.

At the end of each test (at a 100-mm depth), the images of the needle were acquired, elaborated by zooming in on sections of interest, and then the deflections were calculated. A scheme of the protocol tests is shown in Fig. 10a. For each different tension (*Fs*) applied to the stiffening cables, the deflection (*k*) is calculated as the distance between the tip of the

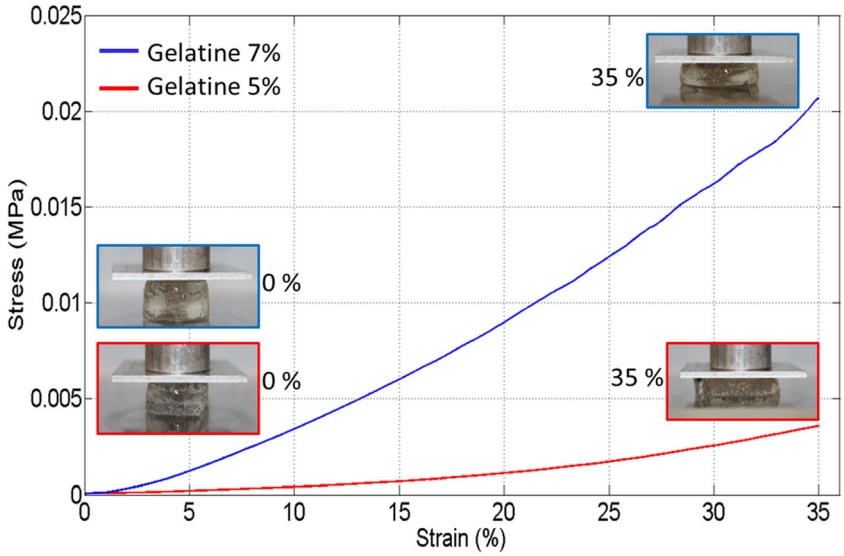

Fig. 9 Stress-strain curves of 5% (red line) and 7% (blue line) gelatine. In the insets, initial and final states of the samples are shown

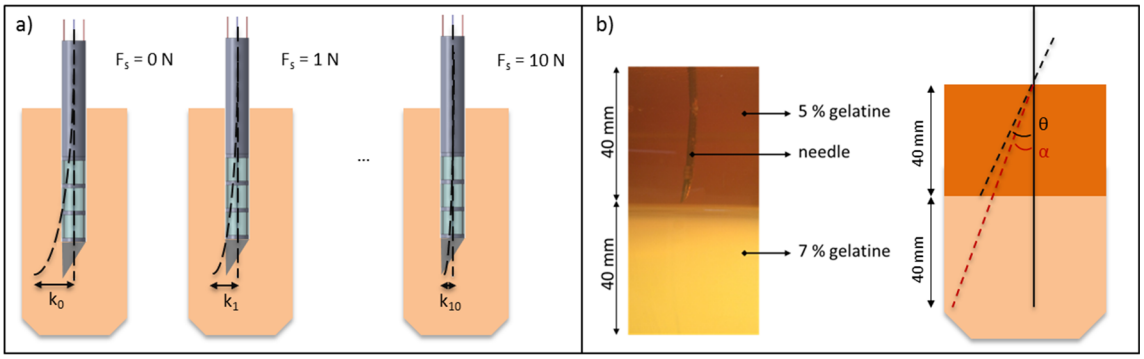

Fig. 10 **a** Protocol for tests in one-layer phantom. The deflection, k, was measured for each different tension state. **b**_left two-layer phantom composed of two 40 mm layers made by 5 and 7% gelatine; **b**_right angles calculated to evaluate the adaptability of the mechanism. θ is the angle between the needle and the vertical axis when the needle is inserted in the 5% gelatine layer at 5 N tension; α is the angle between the needle and the vertical axis when the needle is inserted in the 7% gelatine layer in the range 5–10 N with steps of 1 N

deflected needle and the vertical axis of the needle. It is expected that when tension increases, the deflection decreases. The aim was to quantitatively evaluate the deflection for each tension value in order to understand which tension value could be suitable to approach the target.

1.1.2. Two-layer phantom tests

The setup used for two-layer phantom tests was the same as that of the previous experiment. In this case, the phantom was made of two 40 mm layers characterised by different percentages of gelatine: 5% gelatine on the top and 7% on the bottom (Fig. 10b), which was stiffer than the first layer.

The aim of these tests was to evaluate whether the needle was able to maintain the trajectory in the stiffer layer and for which tension of the variable stiffness mechanism this was possible.

Only the stiffening cables were tensioned, while the driving cables were free to move. Before introducing the needle into the phantom, the stiffening cables were tensioned with 5 N, which represented the minimum suitable value usable in working conditions, as demonstrated by the one-layer phantom tests (see Section 3.2.1). The needle was introduced in the first layer at a speed of 3 mm/s. After the first 40 mm depth, the linear stage was stopped, and the load on the stiffening cables was increased by 1 N. Then, the needle was moved through the second layer at the same speed. For each increment in load, three repetitions were performed at different positions in the phantom so the data would not be affected due to the presence of a previous path. The tests were performed with up to 10 N tension in the second layer. The motion of the needle in the phantom was acquired for each test, and the adaptability of the needle to the stiffer gelatine was evaluated considering the angles shown in Fig. 10b. θ is the angle between the needle and the vertical axis when the needle was inserted in the soft gelatine (first 40 mm), while α is the angle when the needle was inserted in the stiff gelatine. θ was calculated for 5 N tension; thus, it is the same for all tests. α was calculated for each test in the range 5–10 N with steps of 1 N. The aim was to compare the angles, α and θ, and to identify the tension for which the angles were similar in order to evaluate at which tension values the trajectory of the needle was not deviated by the stiffer tissues.

4 Results

4.1 Performance evaluation of the variable stiffness mechanism

4.1.1 Straight position

The force exerted by the variable stiffness mechanism was evaluated for 18 values of tension on the stiffening cables in the range 0–17 N with steps of 1 N and for a 2-mm lateral displacement of the mechanism.

The results are shown in Fig. 11a. Each curve of the graph represents the trend of the force exerted by the prototype for different tensions applied to the cables. When the tension applied to the stiffening cables increased, the force exerted by the prototype increased as well with an approximately linear trend.

When the mechanism was not tensioned, the force exerted at 2 mm of lateral displacement was lower than 0.5 N. For a tension of 9 N, the force exerted by the prototype was 1.3 N, which is a value compatible with the puncturing of some biological tissues. For a tension of 17 N, the force exerted by the prototype was 3.6 N.

In Fig. 11b, three representative positions of the prototype are reported. They are relative to the tensioning states of 0 N (no tension, Fig. 11b (1)), 9 N (first working value, Fig. 11b (2)), and 17 N (the maximum value considered, Fig. 11b (3)). For each case, the simulated deformed mechanism was compared with the experimental one.

The FE simulations reproduced the working principle and the deformations of the mechanism, which was validated by the experimental tests.

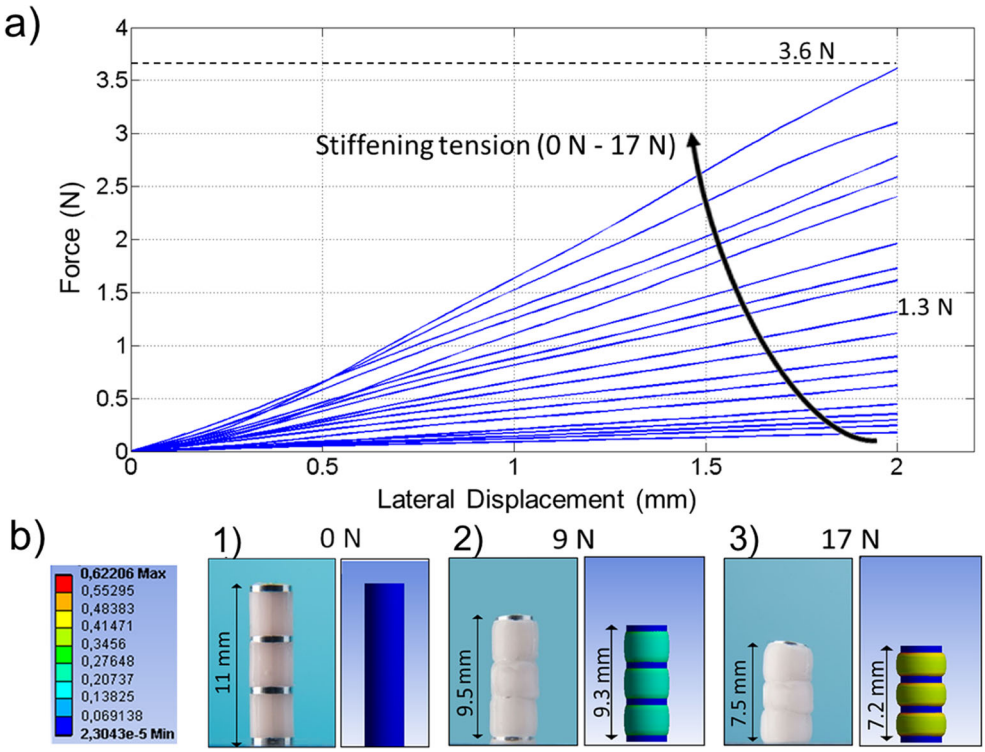

Fig. 11 **a** Average force-lateral displacement curves for the straight position in the range 0–17 N of tension of the stiffening cables ($STD_{MAX} < 0.11$). **b** Strain behaviour of the mechanism in the straight position when it was tensioned with 0 N (1), 9 N (2) and 17 N (3). In each case, the experimental strain (left) and the strain simulated with Ansys Inc. (right) were reported

It is worth mentioning that when the stiffening cables were tensioned, the mechanism was compressed, and its length slightly decreased, while the width of the compliant parts increased. From the experimental results in Fig. 11b, at 9 N tensioning, the length of the prototype decreased by 1.5 mm with respect to the rest position (0 N), while at 17 N tensioning, the length decreased by 3.5 mm. The FE simulations showed the same behaviour with slightly bigger deformations: a 1.7-mm decrease in length @ 9 N, and 3.8 mm @ 17 N.

4.1.2 Curved position

For the straight position, the 20° curved state of the prototype was tested for different tensions in the range 0–17 N. The force-displacement curves are shown in Fig. 12.

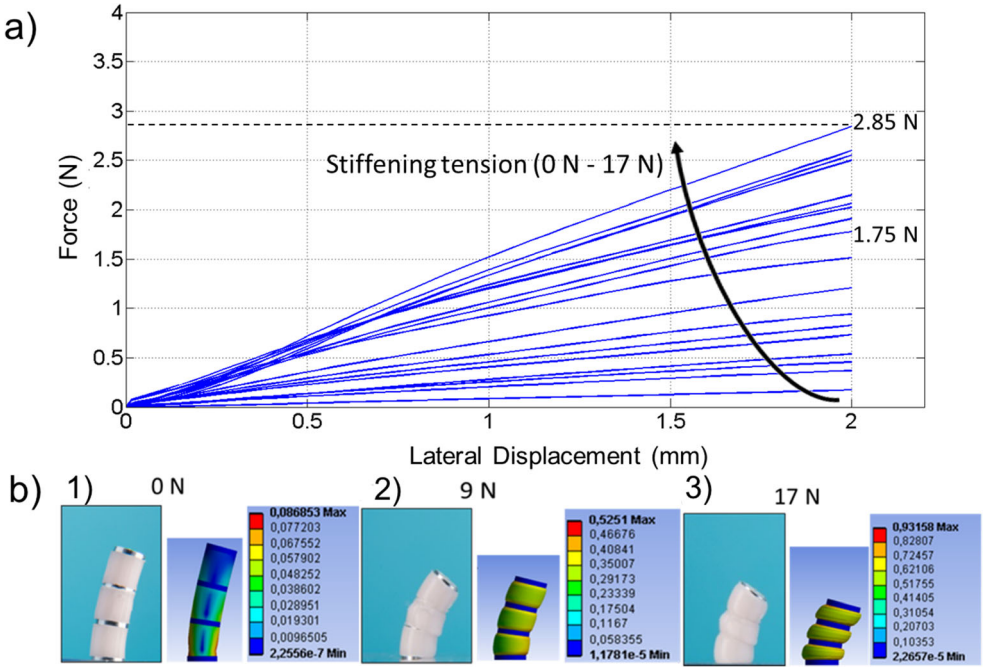

Fig. 12 **a** Average force-displacement curves for the 20° curved position in the 0–17 N range of tension of the stiffening cables ($STD_{MAX} < 0.15$). **b** Strain behaviour of the mechanism in the curved position when it was tensioned with 0 N (1), 9 N (2) and 17 N (3). In each case, the experimental strain (left) and the strain simulated with Ansys Inc. (right) were reported

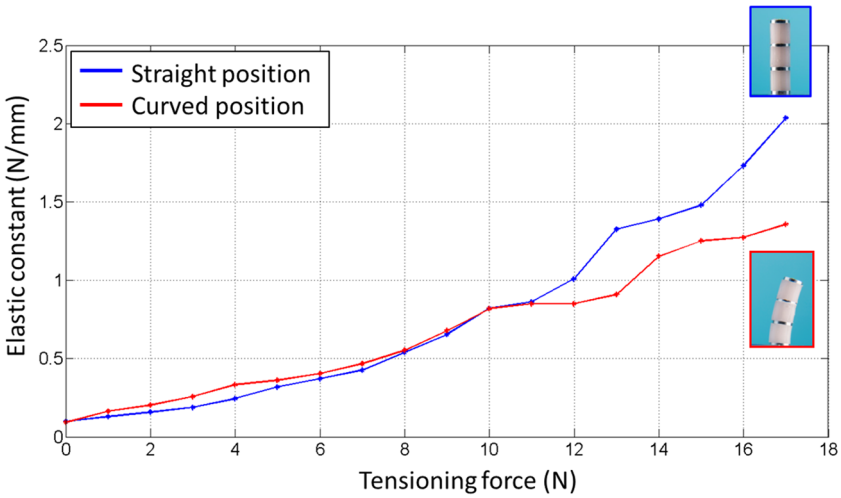

Fig. 13 Elastic constants for the straight (blue line) and curved (red line) positions

Each curve represented the trend of the force exerted by the prototype at a different value of the tension on the stiffening cables. As in the straight position and in this case as well, the trend of the curves was roughly linear, and the exerted tension increased when the stiffening tension increased. When the mechanism was not tensioned, the force exerted was lower than 0.5 N as in the straight position. At 9 N, the force was 1.75 N, which was higher than that in the straight position, while at 17 N, the force was 2.85 N and lower than that in the straight case.

In Fig. 12b, three representative cases of the curved position are shown. They were relative to the 0 N, 9 N and 17 N stiffening tensions. Both the FE simulations and the experimental configurations are reported. For the straight position, the FE-simulated behaviour was validated by the experimental tests. In this case, the strain of the prototype was greater than that in the straight case due to the pre-compression used to maintain the prototype at 20°.

To evaluate the stiffness variation, the elastic constants were calculated as the slope of the linear tracts of the curves. These constants were calculated for all the curves in both the straight and the curved positions, as shown in Fig. 13.

The elastic constant of the curved state (red line) was slightly higher than that of the straight state until 10 N tensioning. After this tensioning, the elastic constants showed different behaviours; the elastic constant relative to the straight position continued to increase, while the elastic constant relative to the curved state increased as well but remained below the curve of the straight state.

The initial tract of the curves until 10 N could be considered the "working window" of the mechanism. In this tract, the elastic constants for both positions were similar, and the trend was approximately linear. For values of tension higher than 10 N, the curve relative to the curved state increased more slowly than that of the other curve, perhaps due to a negative effect of a moment caused by the high tensioning state and the action of the displacement.

4.2 Deflection and stiffness adaptability of the needle

The behaviour of the variable stiffness needle was evaluated in one-layer and two-layer phantoms.

1.1.3. One-layer phantom tests

The needle was inserted in a 5% gelatine phantom, and the deflection was calculated at a 100 mm depth. The results of the deflection are shown in Fig. 14.

Overall, the deflection decreased when the tension on the stiffening cables increased. The deflection was 17.34 mm when the needle was tensioned with 2 N, and it decreased up to 4.4 mm when tensioned with 10 N. For low tensions comprised within the range 2–4 N, the tip did not follow the motion of the cannula, and it seemed to move independently. In addition, the deflection at low tensions had a large variability as indicated by the standard deviations. At 5 N tensioning, the tip moved together with the cannula, and the standard deviation significantly decreased. For these reasons, 5 N tension can be considered as the first working value for the

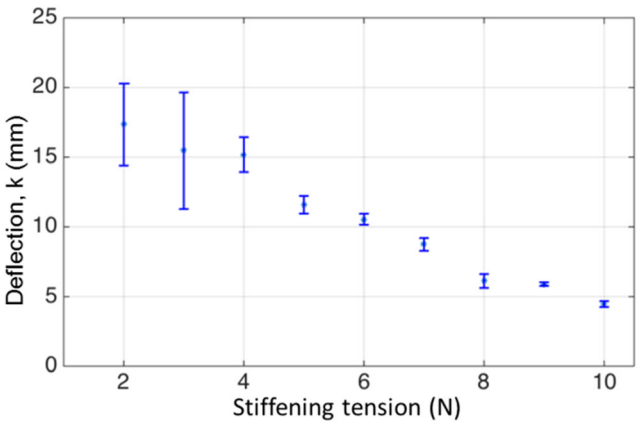

Fig. 14 Deflection values of the needle in a one-layer phantom

presented needle. For higher tension values, both the deflection and the standard deviation decreased, and the device showed a stable behaviour for a needle application.

1.1.4. Two-layer phantom tests

In the case of the two-layer phantom, the needle was inserted in a soft gelatine and then in a stiffer one to evaluate its adaptability to a different stiffness. The θ angle (indicated in Fig. 10b) was calculated at 40 mm in the soft gelatine, and it was 6.6°. To verify the tension at which the trajectory due to the θ angle remained constant in the stiffer gelatine, α angles (indicated in Fig. 10b) were measured for different tension values, as shown in Fig. 15.

When the tension on the stiffening cables was 5 N or 6 N and the tip was not able to follow the cannula into the stiffer layer, α was close to 10°, and the standard deviation was significant. For higher tensions up to 8 N, the tip moved together with the rest of the needle passing through the different layers. However, the trajectory in the stiff layer was different from the trajectory in the softer one; indeed, the α angle was different from θ. In the range 8–9 N, the corresponding α values included the θ value (6.6°), and the tip moved together with the cannula. In this range, it was possible to manage the tension on the stiffening cables so that the same angle was described when the needle moved in the stiffer layer. This indicated a possibility to maintain the same trajectory in a stiffer layer and easily reach the target without unexpected deviations of the needle. For higher stiffening tensions, the values of α were smaller than 6.6°, the trajectory of the needle in the stiffer layer was different, and the deviation was reduced.

5 Discussion

In this work, a variable stiffness mechanism for needles has been presented.

The mechanism was designed and tested to study a new concept of adaptable stiffness to compensate for tissue inhomogeneity during the insertion of medical needles into the human body. This work focuses on the characterisation of the variable stiffness mechanism, which first was studied as a single component and later, after its integration into the needle, was tested in terms of overall behaviour.

The variable stiffness mechanism was integrated in a general-purpose needle in order to assess the success of the integration process. At this level of research, a specific application scenario, such as breast, lung or thyroid, was considered. Optimizations could include a design and control system aimed at a specific application.

Moreover, with regard to the kind of needle and the fabrication process described in Section 2.2, it is worth mentioning that, at this stage of research, the whole variable stiffness mechanism is manufactured as a solid piece without any operative channel. However, the fabrication process described above allows making a hole through the overall mechanism for use in needle biopsies or in fluid sampling procedures [43]. According to Eq. 7, the lumen into the prototype decreases the stiffness of the whole variable stiffness mechanism. The reduction in stiffness can be balanced by pouring a stiffer silicone or braiding the lumen with fibres. Moreover, the lack of a hole in the mechanism makes the needle unusable for clinical applications. Experiments have been carried out to assess the behaviour of the prototype proving the working concept, which has been assessed to work.

Indeed, from the experimental results reported in Section 4.1, it is possible to assess that when the variable stiffness mechanism is tensioned, the developed force increases. As shown in Fig. 11b, when the mechanism is compressed, the length slightly decreases. With the aim to integrate the mechanism in a needle, the reduction in length means a displacement of the tip. If the tip is already moving in the tissues or is close to the target, the displacement of the tip means a loss of position, but this is not an ideal condition during an intervention. However, the mechanism is tendon-driven, and accurate

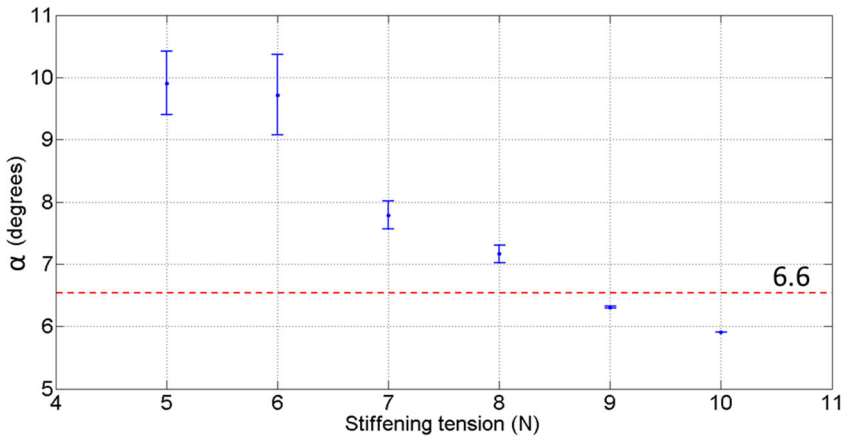

Fig. 15 α angles of the needle in a two-layer phantom

control of the cables and distance of insertion can allow compensation for the displacement of the tip with some repositioning algorithms of the needle. Unlike the variation in length that should be compensated, the radial increment does not change the properties and the behaviour of the needle. The compliance of the material used guarantees the safety of the mechanism. Moreover, the use of a stiffer silicone would allow higher forces to be reached with less tension. Thus, the compression of the mechanism and the displacement of the tip are minimised, as well as the radial increment, and the bending is assured.

With regard to the overall device, the experimental tests (Section 4) assessed that the variable stiffness mechanism is able to vary the performance of the needle. In particular, tests in the one-layer phantom (Section 4.2.1) demonstrated that needle deflection can be varied, activating the mechanism, while tests in the two-layer phantom (Section 4.2.2) showed that the needle is able to adapt its stiffness, maintaining a trajectory.

It is worth mentioning that at this level of research, the cables have been pulled manually. Future works could integrate an encoder able to measure the ΔL (the displacement of the pulled cables) and send this information to a pulling system. Moreover, the feedback of the variable stiffness mechanism is actually based on direct visualisation of the tip. Future research will take into account the possibility of integrating control systems in the needle, such as imaging guidance or real-time sensors, in order to finely adjust the stiffness and accurately reach the target.

6 Conclusion

In this work, a variable stiffness mechanism for minimally invasive tools has been presented and integrated in a medical needle. The mechanism takes advantage of three cylindrical compliant parts alternatively connected in series to four rigid plates. Four cables, symmetrically placed at 90° along the needle diameter, allow the omnidirectional bending of the tip if sequentially tensioned and the tuning of the stiffness if two antagonistic cables are simultaneously tensioned with the same load.

Force tests allowed calculation of the forces developed by the single mechanism at different tensioning states. A tension of 17 N on the stiffening cables allows the mechanism to exert 3.6 N in the straight position and 2.85 N in the curved state. The range of the developed force results was compatible with some needle operations starting at 9 N tensioning states.

The insertion tasks of the overall device in gelatine phantoms, simulating the stiffness of some biological tissues, permitted the evaluation of the behaviour of the needle in working conditions. Tests in a one-layer phantom assessed the possibility of varying the deflection of the needle by changing the tensioning state of the stiffening cables. The deflection was reduced from 11.6 to 4.4 mm in the range 5–10 N. Tests in a two-layer phantom allowed the evaluation of the adaptability of the needle to a different stiffness of the gelatine (from 21 to 80 kPa). By managing the tension on the stiffening cables, it is possible to maintain the same trajectory of the needle in a stiffer layer.

The combined use of the cables to move the tip and to stiffen the needle makes the target approach easier and avoids the rotation of the needle inside the tissues and its removal and re-insertion; thus, the damage to the tissues is reduced.

To perform clinical trials, future works will focus on the introduction of an actuation system for cables and integration of real-time control systems. Moreover, further studies could optimise design and materials in order to improve the relation between the pulling forces on the cables and geometrical variations of the mechanism.

Acknowledgements This research is supported by the Dutch Technology Foundation STW (Project #12709), which is part of the Netherlands Organization for Scientific Research (NWO).

References

1. Abolhassani N, Patel R, Moalle M (2007) Needle insertion into soft tissue: a survey. Med Eng Phys 29:413–431
2. Bishoff JT, Stoianovici D, Lee BR, Bauer J, Taylor RH, Whitcomb LL, Cadeddu JA, Chan D, Kavoussi LR (1998) RCM-PAKY: clinical application of a new robotic system for precise needle placement. J Endourol 12:82
3. Zivanovic A, Davies BL (2000) A robotic system for blood sampling. IEEE Trans Inf Technol Biomed 4(1):8–14
4. Rizun PR, McBeth PB, Louw DF, Sutherland GR (2004) Robot-assisted neurosurgery. Semin Laparosc Surg 11(2):99–106
5. Wei Z, Wan G, Gardi L, Mills G, Downey D, Fenster A (2004) Robot-assisted 3D-TRUS guided prostate brachytherapy: system integration and validation. Med Phys 31(3):539–548
6. van de Berg NJ, van Gerwen DJ, Dankelman J, van den Dobbelsteen JJ (2014) Design choices in needle steering—a review. IEEE/ASME Trans. Mechatronics 99:1–12
7. Zhou Y, Thiruvalluvan K, Krzeminski L, Moore WH, Xu Z, Liang Z (2013) CT-guided robotic needle biopsy of lung nodules with respiratory motion-experimental system and preliminary test. Int J Med Robot 9:317–330
8. Misra S, Reed KB, Schafer BW, Ramesh KT, Okamura AM (2010) Mechanics of flexible needles robotically steered through soft tissue. Int J Robot Res 29(13):1640–1660
9. Abolhassani N, Patel RV (2006) Deflection of a flexible needle during insertion into soft tissue. Conf Proc IEEE Eng Med Biol Soc (EMBS) 1:3858–3861
10. Di Maio SP, Salcudean SE (2003) Needle steering and model-based trajectory planning. Conf Proc Med Image Comput Comput Assist Interv 2878:33–40
11. Kratchman LB, Rahman MM, Saunders JR, Swaney PJ, Webster RJ (2011). Toward robotic needle steering in lung biopsy: a tendon actuated approach. Proc SPIE Int Soc Opt Eng 7964:79641I-796411–79 641I-8
12. Magill J, Anderson B, Anderson G, Hess P, Pratt S (2004) Multi-axis mechanical simulator for epidural needle insertion. Proc Med Image Comput Comput Assist Interv (MICCAI) 3078:267–276

13. Maurin B, Piccin O, Bayle B, Gangloff J, de Mathelin M, Soler L, Gangi A (2004) A new robotic system for CT-guided percutaneous procedures with haptic feedback. Proc Int J Comput Assist Radiol Surg (IJCARS) 1268:515–520
14. Hagmann E, Rouiller P, Helmer P, Grange S, Baur C (2004) A haptic guidance tool for CT-directed percutaneous interventions. Conf Proc IEEE Eng Med Biol Soc (EMBS) 1:2746–2749
15. Hong J, Dohi T, Hashizume M, Konishi K, Hata N (2004) An ultrasound-driven needle insertion robot for percutaneous cholecystostomy. Phys Med Biol 49:441–455
16. Kronreif G, Fürst M, Kettenbach J, Figl M, Hanel R (2003) Robotic guidance for percutaneous interventions. Adv Robotics 17:541–560
17. Ding M, Fenster A (2004) Projection-based needle segmentation in 3D ultrasound images. Comput Aided Surg 9(5):193–201
18. Peters TM (2000) Image-guided surgery: from X-rays to virtual reality. Comput Methods Biomech Biomed Engin 4(1):27–57
19. Gerovichev O, Marayong P, Okamura AM (2002) The effect of visual and haptic feedback on manual and teleoperated needle insertion. Proc Med Image Comput Comput Assist Interv (MICCAI) 2488:147–154
20. van de Berg NJ, Dankelman J, van den Dobbelsteen JJ (2015) Design of an actively controlled steerable needle with tendon actuation and FBG-based shape sensing. Med Eng Phys 37:617–622
21. Patil S, Burgner J, Webster RJ III, Alterovitz R (2014) Needle steering in 3-D via rapid replanning. IEEE Trans Robot 30(4): 853–864
22. Hauser K, Alterovitz R, Chentanez N, Okamura A, Goldberg K (2009) Feedback control for steering needles through 3D deformable tissue using helical paths. Robotics Science and Systems 1:37
23. Minhas DS, Engh JA, Fenske MM, Riviere CN (2007) Modeling of needle steering via duty-cycled spinning. Conf Proc IEEE Eng Med Biol Soc (EMBS) 1:2756–2759
24. Swaney P, Burgner J, Gilbert HB, Webster RJ III (2013) A flexure-based steerable needle: high curvature with reduced tissue damage. IEEE Trans Biomed Eng 60(4):906–909
25. Webster RJ III, Okamura AM, Cowan NJ (2006) Toward active cannulas: miniature snake-like surgical robots. Conf Proc IEEE/RSJ Intell Robot Syst 1:2857–2863
26. Roesthuis RJ, van de Berg NJ, van den Dobbelsteen JJ, Misra S (2015) Modeling and steering of a novel actuated-tip needle through a soft-tissue simulant using Fiber Bragg grating sensors. IEEE Int Conf Robot (ICRA):2283–2289
27. Ko S Y, Frasson L, Rodriguez y Baena F (2011). Closed-loop planar motion control of a steerable probe with a "programmable bevel" inspired by Nature IEEE Trans Robot; 27(5):970–983
28. Terayama M, Furusho J, Monden M (2007) Curved multi-tube device for path-error correction in a needle-insertion system. Int J Med Robot (MRCAS) 3(2):125–134
29. Swaney PJ, Mahoney AW, Remirez AA, Lamers E, Hartley BI, Feins RH, Alterovitz R, Webster RJ III (2015) Tendons, concentric tubes, and a bevel tip: three steerable robots in one transoral lung access system. IEEE Int Conf Robot (ICRA) 1:5378–5383
30. van Gerwen DJ, Dankelman J, van den Dobbelsteen JJ (2012) Needle–tissue interaction forces—a survey of experimental data. Med Eng Phys 34:665–680
31. Kataoka H, Washio T, Audette M, Mizuhara K (2001) A model for relations between needle deflection, force, and thickness on needle penetration. Proc Med Image Comput Comput Assist Interv (MICCAI) 2208:966–974
32. Huber S, Wagner M, Medl M, Czembirek H (2003) Benign breast lesions: minimally invasive vacuum-assisted biopsy with 11-gauge needles patient acceptance and effect on follow-up imaging findings. Radiology 226:783–790
33. De Falco I, van den Dobbelsteen JJ (2015). Variable stiffness mechanism for needles: preliminary study, Proc Design Med Devices (DMD), (16), 35–36
34. Culmone C, De Falco I, Menciassi A, Dankelman J, van den Dobbelsteen JJ (2017) A variable stiffness mechanism for minimally invasive surgical needles. Hamlyn Symp Med Rob(HSMR):7–8
35. Hahn M, Okamgba S, Scheler P, Freidel K, Hoffmann G, Kraemer B, Wallwiener D, Krainick-Strobel U (2008) Vacuum-assisted breast biopsy: a comparison of 11-gauge and 8-gauge needles in benign breast disease. World J Surg Oncol 6:51
36. Venkataraman S, Dialani V, Gilmore HL, Mehta TS (2012) Stereotactic core biopsy: comparison of 11 gauge with 8 gauge vacuum assisted breast biopsy. Eur J Radiol 81:2613–2619
37. Mayer G, Sarikaya M (2002) Rigid biological composite materials: structural examples for biomimetic design. Exp Mech 42:395–403
38. Tanter M, Bercoff J, Athanasiou A, Deffieux T, Gennisson JL, Montaldo G, Muller M, Tardivon A, Fink M (2008) Quantitative assessment of breast lesion viscoelasticity: initial clinical results using supersonic shear imaging. Ultrasound Med Biol 34(9): 1373–1386
39. Okamura AM, Simone C, O'Leary MD (2004) Force modeling for needle insertion into soft tissue. IEEE Trans Biomed Eng 51(10): 1707–1716
40. Simone C, Okamura AM (2002) Modeling of needle insertion forces for robot-assisted percutaneous therapy. Proc IEEE Int Conf Robot Autom 2:2085–2091
41. Webster RJ, Memisevic J, Okamura AM (2003) Design considerations for robotic needle steering. Proc IEEE Int Conf Robot Autom:88–3594
42. Misra S, Reed KB, Douglas AS, Ramesh KT, Okamura AM (2008) Needle-tissue interaction forces for bevel-tip steerable needles. Proc IEEE RAS EMBS Int Conf Biomed Robot Biomechatron:224–231
43. Fischman AM, Epelboym Y, Siegelbaum RH, Weintraub JL, Kim E, Nowakowski FS, Lookstein RA (2012) Emergent embolization of arterial bleeding after vacuum-assisted breast biopsy. J Vasc Interv Radiol 35(1):194–197

Iris De Falco received a master's degree (cum laude) in biomedical engineering from the University of Pisa, Italy, in 2012 and a Ph.D. in biorobotics from The BioRobotics Institute of Scuola Superiore Sant'Anna in Pisa, Italy, in 2016. In 2011, she joined the Scuola Superiore Sant'Anna, focusing her activity on biomechatronic systems and soft robots for minimally invasive surgery and endoscopy. In 2015, she spent time as a visiting researcher at TU Delft (The Netherlands) in the Minimally Invasive Surgery and Interventional Techniques (MISIT) research group working on a variable stiffness needle for percutaneous interventions. Her research contributions were prized with national and international awards.

Costanza Culmone received a master's degree in biomedical engineering from the University of Pisa, Italy, in 2016. She is currently working towards a Ph.D. in biomechanics at the Delft University of Technology in Delft, The Netherlands. Her research interests are in the areas of surgical medical instruments with a focus on steerable and shape memory systems. In 2015, she was an intern in the Minimally Invasive Surgery and Interventional Techniques (MISIT) group at Delft University of Technology.

Arianna Menciassi is Professor of Biomedical Robotics at Scuola Superiore Sant'Anna (SSSA) and a team leader in the "*Surgical Robotics & Allied Technologies*" Area at The BioRobotics Institute. She has a substantial devotion to training and education, both at SSSA and at the University of Pisa, having served as preceptor to 15 postdoctoral associates, 20 Ph.D. students and ~50 graduate degree recipients. Her main research interests involve biomedical robotics, microsystem technology, nanotechnology and micromechatronics, with a special attention to the synergy between robot-assisted therapy and micro-nano-biotechnology-related solutions. She also focuses on magnetically driven microrobots and microdevices, as well as on biomedical integrated platforms for magnetic navigation and ultrasound-based treatments. She is co-author on more than 370 scientific publications (more than 230 in international journals) and 7 book chapters on biomedical robots/devices and microtechnology. She is also inventor on 25 patents, national and international. She served on the Editorial Board of the IEEE-ASME Trans. on Mechatronics, and she is now a Topic Editor in Medical Robotics of the International Journal of Advanced Robotic Systems; she is Co-Chair of the IEEE Technical Committee on Surgical Robotics, and she is the Nanotechnology Technical Committee representative of the steering committee of the IEEE Transactions on Nanobioscience.

Jenny Dankelman is professor in Minimally Invasive Surgery and Interventional Techniques at the Delft University of Technology (DUT). She obtained her degree in Mathematics, with a specialisation in System and Control Engineering, at the University of Groningen in 1984. Her Ph.D. degree on the dynamics of the coronary circulation was obtained at the DUT, in close co-operation with the Academic Medical Centre Amsterdam (AMC). She continued her research at DUT and was awarded the Antoni van Leeuwenhoek chair in 2001. In 2007, she became head of the Minimally Invasive Surgery and Interventional Techniques group (www.MISIT.nl). She is (co-) author of over 180 peer reviewed publications. Between 2010 and 2014, she was head of the Department of BioMechanical Engineering and in 2013, she became Medical Delta professor. Her research focuses on minimally invasive surgery, needle interventions and endovascular interventions. Her research group cooperates with several hospitals: Leiden University Medical Center where she holds a part time professorship position, Erasmus Medical Center Rotterdam and the AMC. Her interests and research projects are in the fields of designing novel medical instruments, haptics, training and simulation systems, and patient safety, with the focus on minimally invasive techniques.

John J. van den Dobbelsteen obtained his degree in Psychophysics in 1998 at the University of Groningen. His Ph.D. was obtained in 2003 in the Department of Neuroscience of the Erasmus MC in Rotterdam for his research into human motor control, motor learning and sensorimotor integration. In 2005, he started as a research fellow in the Department of Biomechanical Engineering at Delft University of Technology. Since 2007, he has worked there as an associate professor in the Minimally Invasive Surgery and Interventional Techniques (MISIT) research group. His research projects focus on the development of instruments for image-guided percutaneous interventions and the study of forces and motion during instrument–tissue interaction in minimally invasive interventions.